The *dna*SET: A Novel Device for Single-Molecule DNA Sequencing

Prashant Mali and Rakesh K. Lal, *Member, IEEE*

***Abstract*—We present the principle of the *dna*SET, a novel device for single-molecule sequence analysis of DNA strands. The central idea is to measure the variations in current through a single electron transistor (SET) as a target DNA molecule slithers through a nanoeye integrated between the SET's floating island and gate. We present a basic but illustrative simulation of the operation, and the results therefrom lead us to conclude that the *dna*SET has a single-nucleotide resolution that enables it to read off the individual bases in a DNA strand. The versatility of this idea makes it suitable for incorporation in other bio-assay tools, and thus the *dna/protein*SET promises to be a powerful direct sensing device for a wide range of applications.**

***Index Terms*—Affinity sensors, deoxyribonucleic acid (DNA), DNA chip/sensors, dnaSET, nanoeye, sequence analysis, single electron transistor (SET), single-molecule sensing, single-stranded DNA (ssDNA).**

I. Introduction

NUCLEIC acid sequence characterization finds widespread use in genomic analysis and medical diagnostics [1]. Sequence analysis is slated to become still more pervasive as its use expands into other applications: applications as diverse as pollution monitoring, where modification of the DNA of a species is used as a measure of the effect of pollutants on an ecosystem, and bio-terrorism alarm systems, where DNA based signatures can be used to quickly and accurately identify biological warfare agents. The growing number of these tests and their wide applicability has stimulated a demand for automated, inexpensive, and standalone miniature platforms. There is thus a huge motivation for conductometric electronic DNA detection schemes as these would be faster and more compact as compared to prevalent tools such as microarrays and gel electrophoresis. Furthermore, a single-molecule DNA analysis scheme which directly probes bases in the molecule would be in addition reagentless and generic in its applicability, and is the goal of the present work.

Successful concept demonstrations have already been made for conductometric electrochemical/electronic sensors. These exploit the complementary binding properties of DNA or RNA, to either get electrochemical/nanoparticle tags near electrodes, or modify the immittance of an electrically active layer. For instance, the preferential attachment of molecular electronic circuit elements in the presence of a target DNA has been used to successfully effect detection, and these approaches have been reviewed in [2]. Changes in ionic conductivity caused by the movement of a DNA or RNA molecule through a nanopore or membrane channel proteins have also been exploited to sense these molecules [3]. In another innovative but sequential approach [4], target DNA strands are first captured in a gap between two electrodes, following which single-stranded DNA (ssDNA) tagged gold nanoparticles are introduced that hybridize to this target. Finally, a gold-promoted reduction of silver is performed that plates silver in the gap thus closing the circuit. Another promising scheme [5], which utilizes conductance variations of doped semiconductor nanowires due to antigen-antibody attachments, could be extended to DNA/RNA assays. Recently, reagentless schemes (based on molecular beacons) have also been developed for DNA detection. Here, hybridization induced conformational changes alter the tunneling distance between an electrode and a redox label thus signaling a hit [6].

The direct sequencing approach is in comparison still in its nascent stages. The primary tools under investigation here are confocal fluorescence microscopy and evanescent mode devices. To amplify and/or probe DNA molecules, the interaction of DNA with naturally occurring proteins is often used in conjunction with these tools. In fact in a recent demonstration, fluorescence microscopy coupled with DNA polymerase activity was used to successfully determine sequence fingerprints up to 5 bp in length [7]. In another recent development, arrays of sensors that are zero-mode waveguides consisting of nanosized holes in a metal film were used. These serve the dual purpose of a reaction chamber and a part of an optical detection system to simultaneously synthesize and monitor the enzymatic synthesis of double stranded DNA by DNA polymerase using fluorescently tagged nucleotides [8].

None of the above techniques attempt to directly read off the base sequence in a DNA strand. To this end we propose the single electron transistor (SET) for DNA, or the *dna*SET, which is the first proposal for a direct single-molecule electronic DNA analysis device. Here, the constituent nucleotides of a strand are individually probed by measuring the variations in SET current accompanying the threading of the DNA molecule through a nanoeye integrated between its gate and floating island (refer to Fig. 1). The SET plays the role of a sensitive electrometer [9] with the SET island being the potential probe, and the nanoeye provides control by constraining the motion of the DNA such that only a few bases are in proximity of the island at each instant of time. The threading is achieved by a voltage-driven migration of the DNA molecule [10]. The scheme allows not only the probing of the sequence of bases in a single strand of DNA, but also an array of other classes of molecules.

Manuscript received December 30, 2003; revised October 5, 2004. The review of this paper was arranged by Editor S. Datta.

The authors are with the Department of Electrical Engineering, Indian Institute of Technology Bombay, Powai, Mumbai 400076, India (e-mail: rla1@ee.iitb.ac.in).

Digital Object Identifier 10.1109/TED.2004.839740

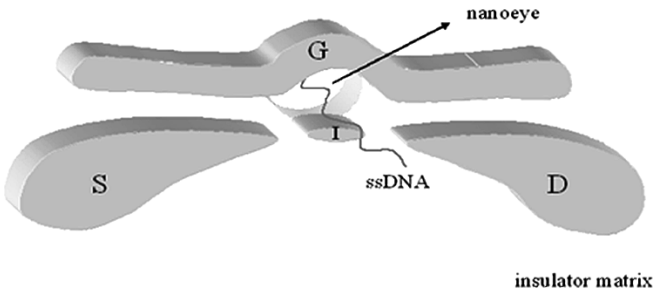

Fig. 1. The *dna*SET: A DNA molecule is seen threading through a nanoeye integrated between the SET island (I) and gate (G).

On account of the differing dielectric properties of the DNA molecule in comparison with the surrounding fluid medium and also due to its spatially varying charge distribution, the process of threading causes both a change in the floating island's self and mutual capacitances, plus also a change in the amount of net induced charge on it. Thus, the sequential threading of the different segments of the molecule (with their differing electrical properties) through the nanoeye, manifests as a time-varying current that is a characteristic signature of the molecule's charge and conformation.

In Sections II–IV, a first-order theoretical simulation of the working of the device is presented. The primary objectives were to check whether the idea works by determining the resolution of the *dna*SET for some typical bio-assay scenarios, and next, to estimate the nature of the current signature when an ssDNA molecule threads through it. Some engineering issues and possible methods for signal amplification have also been discussed.

II. Simulation Approach

Our approach to estimating the *dna*SET current signature for an ssDNA threading experiment is outlined in Fig. 2. The details of the constituent modules are explained next.

A. Structure Used for Simulations

The *dna*SET structure considered for the simulations is based on the fabrication technique proposed in Section IV-C, and is depicted in Fig. 3. The conductors are 1-nm-thick Ti slabs on a SiO_2 layer, with the source-island and the island-drain tunnel junctions being 3 nm in width, and TiO_x as the barrier material (permittivity $\varepsilon_r = 5$ [11], and barrier height $\phi_0 = 0.178$ eV [12]). For simplicity, native Ti oxide formation, and differences in the Ti layer thickness before and after oxidation, have not been considered. The floating island is 3 nm $\times$ 3 nm across, with the edges aligned to the source and the drain. The nanoeye is a nanopore in the oxide, with cross-section 2 nm $\times$ 2 nm and length 10 nm, that opens into two electrolyte reservoirs on either side where electrodes for applying the bias that sets the electrophoretic field for drifting the DNA through the nanoeye are placed (not shown in the figure). The nanoeye center is 1.5 nm away from the island edge. The gate is 3 nm wide and is 7 nm from the island (far enough to have negligible tunnel leakage currents). Finally, the whole structure is covered by a conformally coated Si_3N_4 barrier layer of 0.5-nm thickness (also not shown in the figure). All the simulations have been conducted

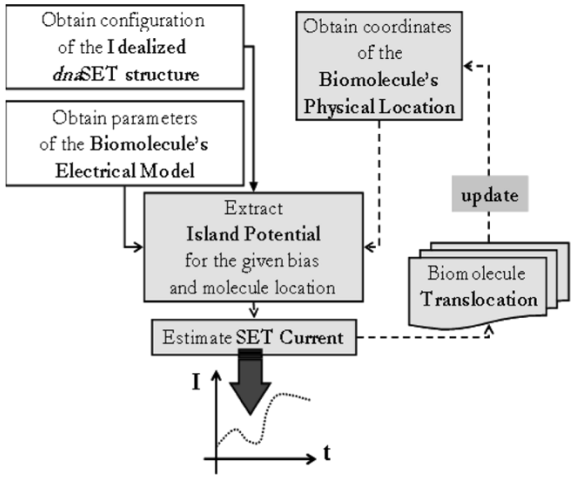

Fig. 2. Simulation flowchart giving the top level approach for the simulations.

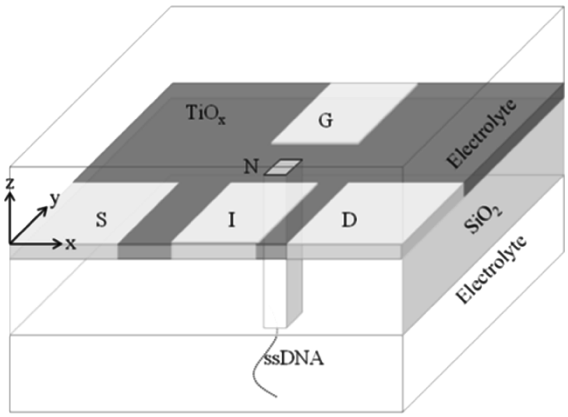

Fig. 3. *dna*SET structure that has been simulated: The source (S), drain (D), island (I), and gate (G), shown in white, are Ti slabs. The dark gray shaded regions correspond to TiO_x. This whole structure is on a SiO_2 base (light gray), which bears a nanochannel (N) that opens on either ends into two reservoirs. An ssDNA is shown threading through the channel from below. (Note: For clarity, the conformal Si_3N_4 coat which covers the SET and the inside walls of the nanochannel have not been shown).

with the nanochannel fluid chosen as water ($\varepsilon_r = 78.4$), and with the electrolyte concentration kept low (much below 0.01 M, the value below which the electrostatic repulsion between the un-neutralized phosphate groups keeps the DNA single strands sufficiently stretched [13]).

B. Electrical Model of ssDNA

To estimate the effect of an ssDNA threading the nanoeye of the *dna*SET on the island potential, we require to first develop an electrical model. This is outlined in the following paragraphs.

Ideally, ssDNA should be modeled as a string of dipoles corresponding to the dipole moments of the constituent nucleotides (these may not necessarily be perfect dipoles), that are further immersed in a flexible non uniform dielectric cylinder of varying ε corresponding to the individual nucleotide polarizabilities (refer to Fig. 4).

However, constrained by the availability of data, we have instead modeled the ssDNA as a dielectric cuboid (of $\varepsilon_r = 1$ and edge $= 1$ nm), which has embedded in it dipoles (of length 1

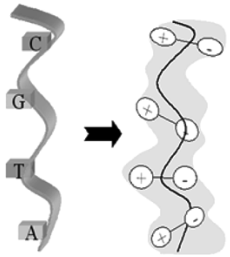

Fig. 4. ssDNA is electrically modeled as a flexible nonuniform dielectric cylinder (shown in light gray), which has embedded in it dipoles that are strung together to form a chain.

TABLE I
ssDNA MODEL PARAMETERS [15],[16]

Base	Dipole Moment (D) – the plane of the dipoles is perpendicular to the sugar backbone.	Orientation relative to the sugar backbone (°) – here 180° implies the positive head of the dipole is nearest to the sugar backbone (this positioning is approximate).
Adenine	2.56	137
Thymine	4.31	285
Guanine	6.65	243
Cytosine	6.49	317

nm) corresponding to the bases alone. Using data from pdb (Protein Data Bank [14]) files the inter-dipole spacing has been approximated as 5 nm (Note: an ssDNA molecule is more flexible and extensible than a dsDNA molecule). The effect of the sugars and phosphates has not been considered, but since the differentiating factor between nucleotides are the bases alone, our goal of estimating the nature of the current signatures is not compromised. The strengths and the relative orientation of the base dipoles were graphically extracted from [15] and [16]. Refer to Table I for details on these parameters.

The theoretical rationale behind this model stems from the observation that while dipole moments are of the order of a few Debye ($\sim 10^{-30}$ Cm), atomic and bond polarizabilities of the constituent atoms and bonds are of the order of $\sim 10^{-40}$ $\mathrm{C^2m^2/J}$. Consequently, the molecular dipole moments will swamp out the effect of any induced dipoles. The experimentally observed macroscopic nucleotide dielectric constants (in the liquid phase) thus are in large part due to the rearranging of molecular dipoles [17]. However, in the case of the *dna*SET, the nano-dimensions of the channel and also the rigidity imposed by the DNA chain, constrains both the number and the motion of the constituent nucleotides in the vicinity of the island. It would thus be incorrect to model a DNA single strand as a chain of dielectric slabs each of a value corresponding to the macroscopic dielectric constants of the constituent nucleotides.

C. Simulator Modules

We assume that the electronic system in the SET relaxes with a time constant that is far smaller than that for a single nucleotide translocation through the *dna*SET. Consequently, as outlined in Fig. 3, our simulations are quasistatic in nature. The presence of the ssDNA in the eye changes the island potential, due to a change of the mutual capacitances of the device and the charge on the molecule. Thus, at each sampling instant for a threading biomolecule:

- we first extract the instantaneous island potential and the instantaneous mutual capacitances of the island to the surrounding conductors;
- next, using the extracted capacitances we obtain the gate voltage (or equivalently, the island charge), that will give the extracted island potential, and thus incorporate the effect of the dipoles on the device parameters (refer Fig. 6);
- using these modified biasing conditions and device capacitances we then obtain the *dna*SET current;
- the ssDNA is then translocated and the process repeated to obtain the current as a function of ssDNA location.

To achieve the above subtasks, the following simulator modules were developed.

1) Capacitance and Voltage Extraction Tool: A finite-difference method (FDM) based three-dimensional (3-D) capacitance and voltage extraction tool was implemented. The former module was required for extracting the mutual capacitances between the SET's island and the surrounding conductors, and the latter for estimating the potential on it in the presence of an ssDNA molecule (as polarization effects due to discrete charges and dipoles are more readily dealt with in this scheme).

The above FDM modules take as input the configuration of the various conductors and dielectrics constituting the *dna*SET. In the case of the voltage extractor, the biasing voltages and the net charge on the target island conductor are also to be specified. The entire system is enclosed in a grounded bounding box, and a uniform 3-D mesh is then used to approximate the whole structure. The two basic equations that are now needed to be solved for are

$$\nabla^2\psi = -\frac{\rho}{\varepsilon} \tag{1}$$

$$\oint D \cdot da = Q_{enc}. \tag{2}$$

We accomplish this using the iterative Jacobi's method [18]. For the voltage extractor, an additional equation of the difference form of the Gauss's law for a bounding surface around the island is also framed to complete the set of conditions required to uniquely solve for the specified inputs. Note that at the dielectric interfaces the difference form of (1) gets modified. The new version can be obtained by applying (2) on a suitable Gaussian box enclosing the relevant mesh point. We have considered a cube for our case (this approach is similar to the one outlined in [19]).

The capacitance extraction module has been verified using benchmark geometries. Refer to Table II for a summary of the comparisons. In general, marginally higher values were obtained. This is because we use a uniform mesh, which requires high mesh densities to adequately handle charge concentration and fields along sharp edges and corners.

For situation-specific validation of the voltage extraction module, refer to Fig. 5. Here A, B, and T are conducting cubes of edges 10 μm, 10 μm, and 2 μm, respectively. T, the target cube whose potential we wish to extract, is placed symmetrically between A and B at a distance of 2 μm from each, and this whole structure is further placed symmetrically

TABLE II
VALIDATION OF THE CAPACITANCE EXTRACTOR

Geometry	Input Configuration	Extracted Capacitance	Capacitance using existing tools / formulae
Parallel plate capacitor	Two 1μm thick parallel plates of 80μm×80μm area separated by a distance of 2μm, and immersed in a dielectric of ε=1. The bounding box is 100μm×100μm×100μm	C_{12}=30fF	C_{12}=28fF
Cube [20]	Unit cube in a 25m×25m×25m box	C_{11}=82pF	C_{11}=73pF

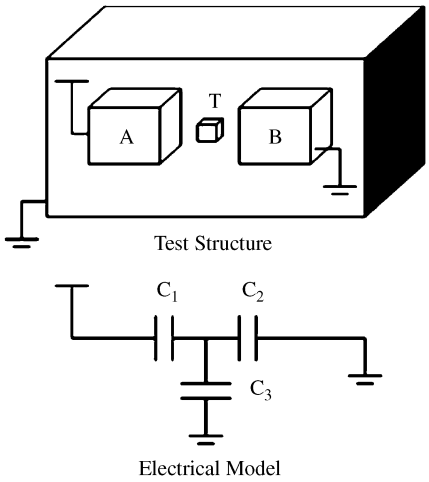

Fig. 5. Structure for testing the potential/voltage extraction module. A, B, and T are conducting cubes in a bounding grounded conducting box and the simulator is validated by checking out convergence and solutions for different boundary conditions and initial guesses.

in a grounded bounding box of edge 50 μm. With A biased at 1 V and B grounded, the extracted potentials on the target T corresponding to some typical scenarios (simulated through the appropriate insertion of dielectrics) were as in Table III.

The capacitance values cited in the table were extracted using the capacitance extraction module. The efficacy of the module working follows from the close match between $C_1/(C_1+C_2+C_3)$ and the extracted potentials in all the above cases.

2) SET Current Estimation Tool: For estimating the current through the *dna*SET (refer Fig. 6 for the electrical model), a SET current simulator was developed. The working of the same was verified against the online simulator at Delft University [21]. The theory behind its working is based on the Orthodox Tunneling Theory [22], which we summarize below.

According to the Orthodox Theory, the tunneling rate across a tunnel junction is given by

$$\Gamma(\Delta F) = \frac{\Delta F}{q^2 R_T \left(1 - \exp\left[\frac{-\Delta F}{kT}\right]\right)}. \quad (3)$$

TABLE III
VALIDATION OF THE VOLTAGE EXTRACTOR

Extracted Capacitance	$V_{T\text{-Guess}}$	$V_{T\text{-Extracted}}$	Remarks
C_1=124aF C_2=124aF C_3=8.7aF	0V	0.48V	matches with the expected value
C_1=124aF C_2=124aF C_3=8.7aF	10V	0.48V	confirms convergence to unique solution
C_1=215aF C_2=120aF C_3= 7.9aF	0V	0.63V	increase is in proportion to the new capacitance values

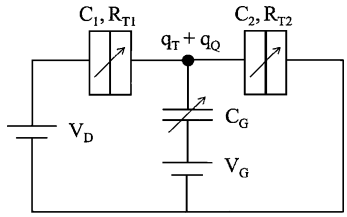

Fig. 6. *dna*SET electrical model: The tunnel junctions are characterized by a tunnel resistance R_T and capacitance C [23]. Here q_T represents the excess island charge due to the tunneling electrons. The effect of DNA threading is manifested through the modulation of the mutual capacitances, primarily C_g, but also C_1 and C_2, and the net island charge (through induced charges q_Q).

Here, ΔF is the energy released at the tunneling junction and is given by [24]

$$\Delta F = \frac{e}{2}(V_{jb} + V_{ja}) \quad (4)$$

where V_{jb} and V_{ja} are, respectively, the voltage across the junction before and after a tunneling event. R_T in (3) is the resistance associated with the tunnel junction and is estimated using the Simmon's formulae in [25]. It is calculated using the junction areas for the device structure from Fig. 3, and the junction material parameters from [11] and [12]. This estimate of tunnel resistance is expected to be on the higher side, as in-elastic tunneling has not been accounted for.

III. RESULTS

The simulations have been carried out in two parts. In the first round, the sensitivity of the *dna*SET to changes in permittivity, charge, and position of a nano-particle simulating a biomolecule is determined, and in the next a few ssDNA threading runs are simulated. In the Section IV we then discuss the issues concerning *dna*SET noise, and outline a general approach for the de-convolution of the current signature in an actual sequencing scenario.

The enclosing bounding box size for the simulation of the structure in Fig. 3 was taken as 40 nm. Note that the fields due to translocation electrodes have not been considered. This simplification is justifiable since their inclusion (and also that of the effect of the sugars and phosphates into the ssDNA model) would only add a constant term to the extracted potential at each sampling instant, and thus just shift the resulting signatures.

The extracted mutual capacitances for the *dna*SET structure were as follows: $C_{\text{island}} = 2.3$ aF, $C_{\text{island-drain}} = C_{\text{island-source}} = 0.66$ aF, $C_{\text{island-gate}} = 0.53$ aF, and

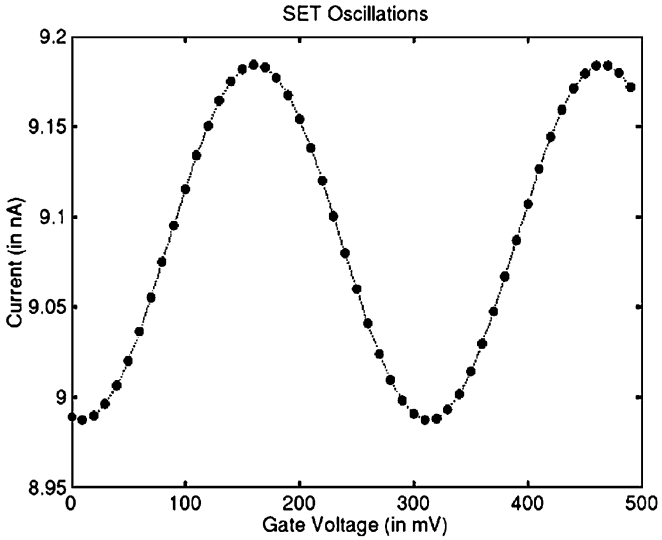

Fig. 7. I_D-V_G plot for the *dna*SET: Here $V_D = 0.01$ V, $T = 280$ K, and estimated tunneling resistance is ~ 346 kΩ for each junction.

$C_{\text{island-bounding box}} = 0.44$ aF. The resulting I_D-V_G plot (depicting the characteristic SET oscillations) is shown in Fig. 7.

Selection of geometric parameters and biasing voltages were governed by the following considerations.

- Firstly, we need a very low value of the island capacitance to observe room temperature SET oscillations. This requires the island size to be small (< 10 nm diameter). Further, a large capacitance (and/or an island size) would reduce the *dna*SET resolution (i.e., the change in the island potential ψ_I) as

$$\delta\psi_I \propto \frac{\delta Q}{C_{\text{island}}}. \tag{5}$$

  And given fixed tunnel distance, C_{island} depends on the surface area of the island and thence island size.
- Next, the mapping from molecule location (i.e., island potential) to SET current depends on the magnitude and slope of the I_D-V_G plot. Specifically, the magnitude (I_D) is affected by the tunnel resistances, and the slope (dI_D/dV_G) is affected by the biasing, mutual capacitances, and temperature of operation. Thus, in general lower resistances, lower capacitances and as low a temperature of operation as feasible are preferred. Furthermore, the quiescent bias should be such that device is biased to realize the maximum slope of the transfer characteristic.
- Finally, to reduce the effect of the bounding box one would ideally prefer to have the input structures nested deep inside it. However, as we have employed uniform meshing, this approach would substantially increase the mesh density and hence prohibitively increase the computation time. To mitigate this computational cost, we have immersed the device in a nonuniform medium—*viz*, we have plastered the inside walls of the bounding box by a very low k fictitious dielectric material ($\varepsilon_r = 0.1$ and thickness $= 1.5$ nm). This has the effect of increasing the effective size of the bounding box (and is in fact equivalent to nonuniform meshing). A first-order one-dimensional (1-D) analysis predicts an increase in the box edge to be of the order of $\sim t \times (\varepsilon/\varepsilon_{\text{pseudo}} - 1)$, where t is the thickness of the pseudodielectric.

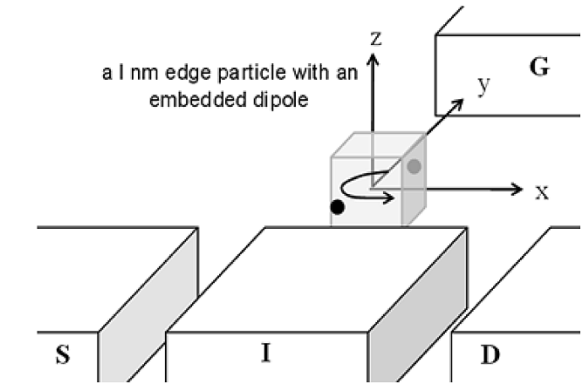

Fig. 8. Test dielectric nanoparticle, simulating a molecule, between the gate and the island, and its translation directions and internal dipole orientations for which simulations were made (Note: for clarity, structural details such as the nanochannel and the electrolyte reservoirs have not been shown).

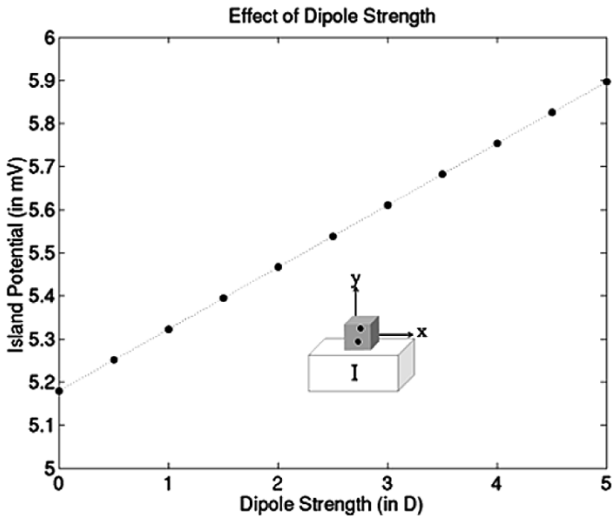

Fig. 9. ψ_I versus dipole strength: Plot of the island potential with respect to changes in the strength of the particle's dipole strength—note that the potential increases linearly with dipole strength.

A. *dna*SET Resolution

The resolving power of the *dna*SET was tested using a dielectric cube of edge 1 nm and $\varepsilon_r = 1$ with a dipole embedded in it (refer Fig. 8). This in a sense can be considered to be a generalized electrical model for bio-molecules of this size.

The spatial position of the particle, and its dipole orientation and strength was varied to observe how the *dna*SET's island potential changed ($V_D = 0.01$ V, $V_G = 0.01$ V, and $T = 280$ K). The results obtained are shown in Figs. 9–11, and they underline the high sensitivity of the *dna*SET, which is seen to readily distinguish such variations. Note that in all the simulation runs, the test particle center is at a distance of 1.5 nm from the island and its position and alignment is symmetrical and parallel with respect to the island's zx surface. Also, the default test particle dipole strength is taken as 2.5D, with the positive head of the

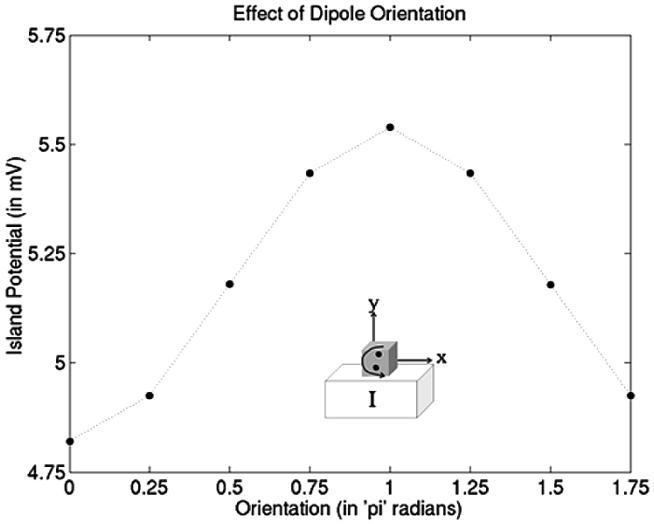

Fig. 10. ψ_I versus orientation: Plot of the island potential with respect to changes in the orientation of the particle's dipole moment (angles are in π radians). Observe that as expected the island potential peaks when the positive head of the dipole is nearest to it.

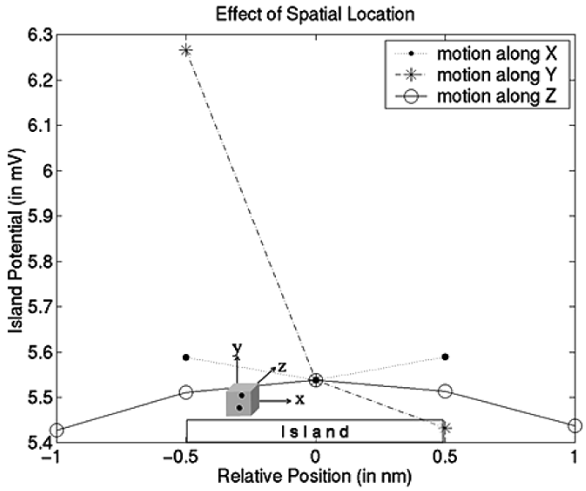

Fig. 11. ψ_I versus position: Plot of the island potential with respect to changes in the spatial location of the particle in the nanochannel. The default position of the particle center is 1.5 nm above the island in the nanoeye, and in each of the three simulation runs it is displaced in either of the x, y, or z directions. Observe that the island potential drops sharply as the particle is taken farther away (along the y axis) from it. However, movement along the x and z axes results in a relatively much lesser change.

dipole facing the island, and the dipole axis lying perpendicular to the zx surface.

B. ssDNA Threading

In this subsection, we report the results of simulations for ssDNA molecules threading the nanoeye. The simulations show that drain current versus time would give the signature of the molecule threading through. In these simulations, 10-base strands were moved along a straight-line path through the nanoeye (SET bias: $V_D = 0.05$ V, $V_G = 0.122$ V; and $T = 280$ K). The traversed path is symmetrical to the zx surface of the island, with the strand being at a distance of 1.5 nm from it. Further, the bases face the island and do not change their relative orientations from the ones specified in Table I.

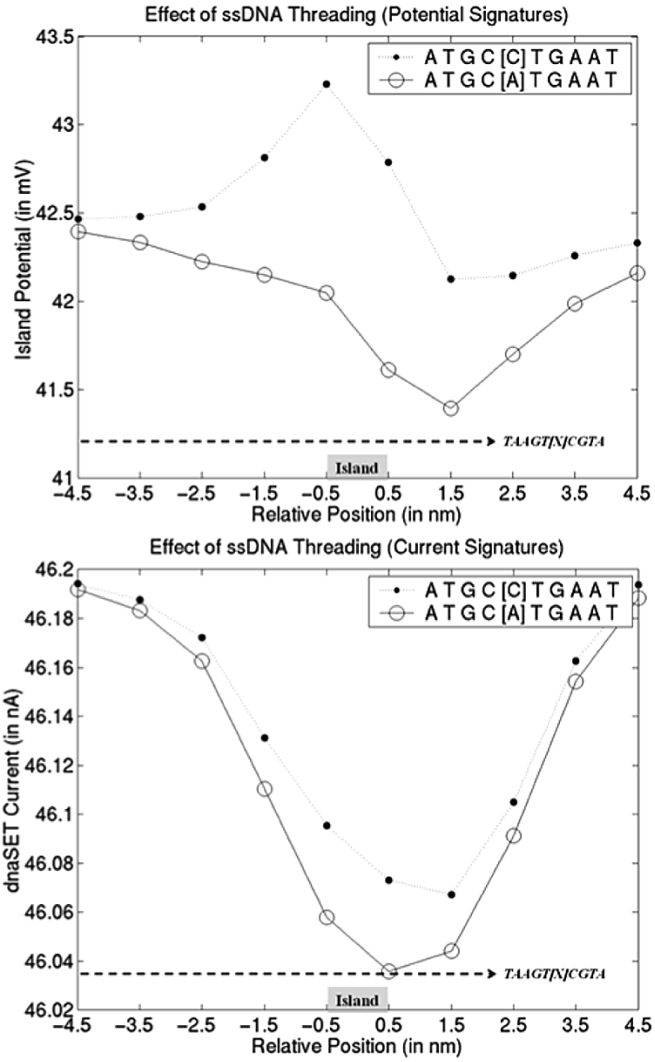

Fig. 12. The *dna*SET potential (top) and current signatures (bottom) when ssDNA thread through the device. Note that the two current curves are distinct ($\Delta I_D \sim 37$ pA).

Note that the island edge is 1 nm thick and the 10-base ssDNA is 5 nm long. While the island potential cannot be directly probed, the SET current can be measured and current versus time can be a signature for an ssDNA threading through the nanoeye. The resulting plots are shown in Fig. 12. Here, the x axis values give the relative position (with respect to the island) of the fifth base in the chain at each sampling instant. Note that a single change in a nucleotide (from C to A above) results in a decipherable change in the plots ($\Delta I_D \sim 37$ pA), and these can thus be used to effectively distinguish one strand from the other.

To determine the resolution of the *dna*SET, another set of simulations was performed, wherein a 10-base strand of all A's was threaded through the *dna*SET and the SET current obtained. Next the fifth base in the strand was replaced in three successive runs to T, G, and C. The peak current differences obtained were 16.5 pA (T for A), -6.3 pA (G for A), and 36.8 pA (C for A) respectively.

In summary, for the *dna*SET simulated, the drain current changes by about 150 pA in 50 nA when an ssDNA threads

through the device, and by about 10 pA for a single base mismatch at the center of decamer strands.

IV. Discussion

A. Noise

Noise in SETs is an important consideration for operation at room temperature and would also be so for the *dna*SET. SETs have both flicker and white noise components. For SETs made of high conductivity metals and trap-free dielectrics, the white noise floor lies between the quantum noise limit and the Schottky shot noise limit as the temperature of operation is raised from milli-Kelvin to room temperature. If the spectral density of the drain current noise is approximated by the Schottky formula $2eI$ [26], for the structure simulated in this work, the root mean square (rms) drain current noise is estimated to be ~ 3.9 pA ($V_D = 0.05$ V, $T = 280$ K, $R_T = 346$ kΩ, and bandwidth $= 1$ kHz). In practice, the *dna*SET would need to be operated above the $1/f$ noise corner frequency by ensuring that the transit velocity of the molecule is above a certain threshold. One would require a current source and a source follower or a microwave reflection measurement setup, as in the case of an RF-SET [9], followed by a bandpass filter of the appropriate bandwidth. The lower cutoff frequency should be above the noise corner frequency and the upper cutoff chosen to limit the rms value of the system noise. The lower cutoff frequency imposes a limit to the number of bases that can then be of the same type and the upper cutoff frequency sets the maximum transit velocity.

For a *dna*SET there would be other sources of noise too, such as due to change of surface charge or the drift or diffusion of an ion in the nanoeye, plus the noise of the low noise amplifier following it. These can be overcome by scaling down and optimizing the *dna*SET geometry, using better signal processing algorithms, and/or the use of a solvent that has a lower freezing point.

B. Signal De-Convolution

The *dna*SET could be used in two modes: sensor mode and sequencer mode. In the sensor mode, one would obtain the signature of a target molecule that needs to be sensed, either by simulation or by carrying out a run with the target molecules and capturing their signature, and then using that for checking out whether signals from analyte molecules are similar. For sequencing, one would need to match the signal with those that would arise from probable sequences and choose that sequence which gives the best match. Needless to say, the signal matching would have to be done with a digital correlator to reduce the effects of noise, with the possibility of using adaptive algorithms to remove the effect of ions and/or surface trapping and de-trapping.

The correlation algorithm can however be speeded-up for the *dna*SET. Since the bases in the threading ssDNA approach the island sequentially and only nucleotides within a limited distance about the island make a noticeable contribution to the island's potential, one can use a sliding window adaptive correlation algorithm. One can start to guess and validate the guess from the instant molecules enter the sensing zone, and subsequently use that guess and the current reading to both predict the next nucleotide in the sequence and also to improve on the estimates for the past ones. However, this simple signal de-convolution would be complicated by the finite size of the island, and also the random paths that a threading strand could take as it traverses the nanoeye. In particular, it is clear from Fig. 11 that the island potential is very strongly dependent on the physical location of the biomolecule (especially with regards to position along the y direction). This problem can, however, be largely alleviated by using narrow rectangular/ellipsoidal nanoeye cross-sections. But in general, this random motion would induce deviations in the above plots, which would thus need to be accounted for before interpretation is possible. A possible way out would be to modify the de-convolving algorithm by programming it to exploit the rigidity of the ssDNA chain and the fixed inter-nucleotide spacing to reduce the number of possible physical locations that adjacent nucleotides in a strand may take. This would thus help reduce the number of paths that a threading strand may have traversed.

C. Fabrication

We do realize that the fabrication of the *dna*SET is a technology challenge. However, modern nanofabrication tools provide the possibility of fabricating such a structure as demonstrated by Gotoh *et al.* [11] and Klein *et al.* [27], wherein innovative scanning probe based anodic oxidation and nanocrystal growth have been used for the fabrication of room temperature SETs. A possible approach using the former scheme would be as follows: A nanopore (~ 3–4 nm across) is first machined in a thin SiO_2 layer (~ 10–15 nm) supported on a silicon substrate. This could be done by using a scanning transmission electron microscope to irradiate a nanometer-sized spot with a focused electron beam (energy ~ 30 KeV, and dose ~ 1 C/cm^2). Electron beam irradiation of SiO_2 causes surface oxygen desorption and the creation of stable bulk vacancies and hydrofluoric acid (HF)-based etchants, which are known to be sensitive to oxide defects, exhibit enhanced etch rate in these exposed regions [28]. Thus, a timed HF etch following the bombardment will yield the desired pore. Subsequently, an ultra thin Ti film is deposited (thickness ~ 2 nm, out of which about 1 nm would get converted to native oxide). The dimensions of the pore opening being larger than the film thickness would ensure that it does not get clogged. A STM tip could then be used to locate the pore, and selectively anodically oxidize the Ti about it and between every electrode pair, including the island, with the patterned island dimensions being of the order of 3 nm $\times$ 3 nm $\times$ 1 nm, and the overall configuration such that the pore is sandwiched between the gate and the floating island. Finally, a thin (~ 0.5 nm) barrier layer of silicon nitride or alumina could be conformally deposited all over (using a technique such as ALD). The resultant device would be a room temperature SET bearing a nanoeye—essentially the idealized *dna*SET structure proposed in this paper.

D. Other Issues

ssDNA transport through the nanoeye could be done hydrostatically or electrophoretically. Application of voltage across the nanoeye affects the potential on the island and hence the biasing of the SET. One would thus need to apply this voltage in a

balanced fashion so that the island potential is not changed. Alternatively, to reduce this effect one may instead use an array of electrodes on either side of the nanochannel that are successively pulsed in pairs (and with opposite but now relatively much reduced voltages) to push and pull the ssDNA along its path.

Also, the actual distribution of energy levels on the island must be taken into account to obtain a more correct current signature. In fact, the nonuniform energy distribution would actually improve the *dna*SET resolution.

Finally, the tunneling resistances and capacitances can be substantially reduced by using materials with still lower barrier heights (the latter as the conductors can now be more widely spaced). Some possibilities include Pb/Cr_2O_3 and Cr/Cr_2O_3 as discussed in [29].

V. Conclusion

Most existing bio/DNA-sensors are fundamentally indirect in principle i.e., they either rely on tags and/or on the basic hybridization/affinity property of probe or target biomolecules to effect detection. While these are very effective schemes, they do not directly probe the target biomolecule electrically, and thus offer little or no direct information of their charge and conformation. In this work, we have proposed and analyzed a new sensing device, the *dna*SET that has a nanoeye placed between the gate and floating island of a SET. When an analyte molecule threads through the nanoeye, its charge and dielectric constant changes the island's potential and thence the SET current, allowing direct electronic sensing of biopolymers from their current signatures.

We show from simulations that for a single stranded DNA molecule threading the device the current changes are of order of 150 pA, and it is possible to get a change of current of ~ 10 pA for a single base difference. This is above the 3.9-pA rms intrinsic device noise of the SET for a 1-kHz signal bandwidth and can be used to therefore distinguish strands even with single base mismatches. With appropriate signal deconvolution algorithms it should be possible to get the sequence of bases as a single-stranded DNA threads through the nanoeye. While we have carried out simulations for single-stranded DNA, the sensing approach can be extended to other classes of molecules. The *dna*SET thus has the capability to probe the electrical parameters of single analyte molecules, giving pointers to the biomolecule's approximate shape, structure dynamics and charge distribution, and thus has the potential to be a generic tool for both sensing and exploration (for example studying molecule conformation changes in a field or affinity processes between molecules).

However, several challenges for fabricating the structure and optimizing the detection protocol need to be addressed before the *dna*SET becomes a reality. These challenges are surmountable and possible methods of signal conditioning and sequence extraction have been discussed.

References

[1] S. Gottleib, "The coming biochips boom: Gene chips go clinical," *Gilder Biotech Rep.*, vol. 1, 2001.

[2] T. G. Drummond, M. G. Hill, and J. K. Barton, "Electrochemical DNA sensors," *Nature Biotechnol.*, vol. 21, pp. 1192–1199, 2003.

[3] H. Wang and D. Branton, "Nanopores with a spark for single-molecule detection," *Nature Biotechnology*, vol. 19, pp. 622–623, 2001.

[4] S. J. Park, T. A. Taton, and C. A. Mirkin, "Array-based electrical detection of DNA with nanoparticle probes," *Science*, vol. 295, pp. 1503–1506, 2002.

[5] Y. Cui, Q. Wei, H. Park, and C. M. Lieber, "Nanowire nanosensors for highly sensitive and selective detection of biological and chemical species," *Science*, vol. 293, pp. 1289–1292, 2001.

[6] C. Fan, K. W. Plaxco, and A. J. Heeger, "Electrochemical interrogation of conformational changes as a reagentless method for the sequence-specific detection of DNA," *Proc. Nat. Acad. Sci.*, vol. 100, no. 16, pp. 9134–9137, 2003.

[7] I. Braslavsky, B. Hebert, E. Kartalov, and S. R. Quake, "Sequence information can be obtained from single DNA molecules," *Proc. Nat. Acad. Sci.*, vol. 100, pp. 3960–3964, 2003.

[8] M. J. Levene, J. Korlach, S. W. Turner, M. Foquet, H. G. Craighead, and W. W. Webb, "Zero-mode waveguides for single-molecule analysis at high concentrations," *Science*, vol. 299, pp. 682–686, 2003.

[9] R. J. Schoelkopf, P. Wahlgren, A. A. Kozhevnikov, P. Delsing, and D. E. Prober, "The radio-frequency single electron transistor (RF-SET): A fast and ultra sensitive electrometer," *Science*, vol. 280, pp. 1238–1242, 1998.

[10] A. Meller, L. Nivon, and D. Branton, "Voltage-driven DNA translocations through a nanopore," *Phys. Rev. Lett.*, vol. 86, pp. 3435–3438, 2001.

[11] Y. Gotoh, K. Matsumoto, T. Maeda, E. B. Cooper, S. R. Manalis, H. Fang, S. C. Minne, T. Hunt, H. Dai, J. Harris, and C. F. Quate, "Experimental and theoretical results of room-temperature single-electron transistor formed by the atomic force microscope nano-oxidation process," *J. Vac. Sci. Technol. A*, vol. 18, pp. 1321–1325, 2000.

[12] B. Irmer, M. Kehrle, H. Lorenz, and J. P. Kotthaus, "Fabrication of Ti/TiO_x tunneling barriers by tapping mode atomic force microscopy induced local oxidation," *Appl. Phys. Lett.*, vol. 71, pp. 1733–1735, 1997.

[13] D. Freifelder, "Structure of denatured DNA," in *Molecular Biology*. Boston, MA: Jones & Bartlett, 1987, pp. 94–95.

[14] (2004) The RCSB Protein Data Bank. [Online]. Available: http://www.rcsb.org/pdb/index.html

[15] J. Sponer, J. Leszczynski, and P. Hobza, "Nature of nucleic acid-base stacking: Nonempirical ab initio and empirical potential characterization of 10 stacked base dimers. Comparison of stacked and H-bonded base pairs," *J. Phys. Chem.*, vol. 100, pp. 5590–5596, 1996.

[16] ——, "Structure and energies of hydrogen-bonded DNA base pairs. A nonempirical study with inclusion of electron correlation," *J. Phys. Chem.*, vol. 100, pp. 1965–1974, 1996.

[17] P. Debye, "Polarization by orientation. Effect of temperature," in *Polar Molecules* New York: Dover, 1929, pp. 27–30.

[18] J. Demmel. (2004) Solving the Discrete Poisson Equation Using Jacobi, SOR, Conjugate Gradients, and the FFT. [Online]. Available: http://www.cs.berkeley.edu~demmel/cs267/lecture24/lecture24.html

[19] J. A. Greenfield and R. W. Dutton, "Nonplanar VLSI device analysis using the solution of Poisson's equation," *IEEE Trans. Electron Devices*, vol. ED-27, pp. 1520–1532, 1980.

[20] D. Reitan and T. Higgins, "Calculation of the electrical capacitance of a cube," *J. Appl. Phys.*, vol. 22, pp. 223–226, 1951.

[21] (2004) Analysing Single Electron Transistor Networks. Delft Univ., Delft, The Netherlands. [Online]. Available: http://vortex.tn.tudelft.nl/research/set/setnets/setnets.html

[22] K. K. Likharev, "Single electron devices and their applications," *Proc. IEEE*, vol. 87, pp. 606–632, Apr. 1999.

[23] M. H. Devoret, D. Esteve, and C. Urbina, "Single-electron transfer in metallic nanostructures," *Nature*, vol. 360, pp. 547–553, 1992.

[24] R. H. Klunder and J. Hoekstra, "Energy conservation in a circuit with single electron tunnel junctions," in *Proc. IEEE Int. Symp. Circuits and Systems*, 2001, pp. 591–594.

[25] J. G. Simmons, "Generalized thermal J-V characteristic for the electric tunnel effect," *J. Appl. Phys.*, vol. 35, pp. 2655–2658, 1964.

[26] A. N. Korotkov, "Intrinsic noise of the single-electron transistor," *Phys. Rev. B*, vol. 49, pp. 10 381–10392, 1994.

[27] D. L. Klein, R. Roth, A. K. L. Lim, A. P. Alivisatos, and P. L. McEuen, "A single-electron transistor made from cadmium selenide nanocrystal," *Nature*, vol. 389, pp. 699–699, 1997.

[28] T. W. O'Keeffe and R. M. Handy, "Fabrication of planar silicon transistors without photoresist," *Solid State Electron.*, vol. 11, pp. 261–266, 1968.

[29] S. Altmeyer, B. Spangenberg, and H. Kurz, "A new concept for the design and realization of metal based single electron devices: Step edge cut-off," *Appl. Phys. Lett.*, vol. 67, no. 4, pp. 569–571, 1995.

Prashant Mali received the B.Tech. and M.Tech. degrees in electrical engineering from the Indian Institute of Technology, Bombay, India, in 2003. He is currently pursuing the Ph.D. degree in biomedical engineering at the Johns Hopkins University, Baltimore, MD.

His research interests include nanofabrication, biosensors, and molecular biology.

Rakesh K. Lal (M'98) received the B.Tech. degree in electronics and communication engineering (Hons.) from the Indian Institute of Technology (IIT), Kharagpur, India, the M.D. degree in electronics from NUFFIC, The Netherlands, and the Ph.D. degree in electrical engineering from IIT, Kanpur, India.

He has been on the faculty of IIT, India since 1984 and is a Professor of electrical engineering. He has been actively involved with the engineering curricula development, has contributed to structural advancement of undergraduate and graduate programs, and has designed and taught courses spanning devices to biosensing microsystems. He has been a Consultant to industry, advising engineering teams on design and prototyping of computer-aided measurement systems for the power industry, yarn testing, particle and cell sizing and characterization, single-cell electroporation, and sensor electronics. He has given process integration and test advise to an industry-research-institute consortium for fabricating high-energy radiation and particle detectors for CERN, and advised the Government of India on Computer and Electronics policies. His research interests include the physics and modeling of semiconductor devices and systems; radiation and high-field effects in MOS, bipolar and heterostructure devices and circuits; and instrumentation for device characterization. He has also been working on radiation sensors, biosensors, and biosensing systems. Over the last decade, much of the biosensors research has evolved into microfabricated biosensing systems for bio-object assay and manipulation, that have included developing and understanding systems for micro-capillary electrophoresis, single-cell electroporation, chemotactic sensing, and affinity sensor arrays.